Laboratory report
Digital Imaging
Group 25

Rocco Ardino
Matr. 1231629

Francesco Gentile
Matr. 1239149

Matteo De Tullio
Matr. 1225015

24-28-29 October 2019

1 Objectives

- Measurement of the mass attenuation coefficient of different materials for a 511 keV photon beam emitted by a ^{22}Na γ-ray source.
- Construction of the digital image of an unknown object inside a black box and study of its material composition.

2 Experimental apparatus

The instrumentation used in order to perform the experiment includes:

- samples of different materials, namely **lead**, **polyethylene**, **aluminium**, **iron** and **graphite**.
- A ^{22}Na γ-rays source, placed into an iron collimator, which provides a photon beam with a defined collinear geometry.
- 8 detectors, denoted as **D1-D8**, consisting of scintillator crystals of Bismuth Germanate $B_4Ge_3O_{12}$ with a size of 18 x 15 x 25 mm^3 (where the thickness is 25 mm) and Hamamatsu photomultipliers R4124, which perform the readout. The first one is placed on one side of the collimator while the 7 left are collected into a linear array which is located in the opposite direction.
- A motorized slide equipped with step-by-step engine, with the function of moving the samples. It can be controlled via PC through a browser.
- The electronics involved in this experiment is made out of a Tektronix TDS 1002B oscilloscope, a unit of Power Supply CAEN N472, a variable gain amplifier PHILIPS 777, a fast discriminator CAEN N413 and a constant Fraction Discriminator ESN CF 8000.
- The acquisition system uses two digitizers, called respectively A and B, each one provided of four channels, labelled with numbers from 0 to 3.

3 Calibration of the detectors

Data Acquisition This phase of the experiment has been performed when there was no material between the ^{22}Na source and the array. First of all, we proceeded in connecting the gain amplifier to the oscilloscope and then noted roughly the order of magnitude of the amplitude and rise time of the signal for each detector. It was crucial to set the CFTD threshold to the minimum value needed to cut the noise and trigger on the falling edge of the signal.
The typical shape of a ^{22}Na γ-spectrum shows two remarkable peaks as energy increases: the first at 511 keV, which is actually preceded by a Compton edge, and the other one at 1275 keV. A lot of effort has been put, again, in checking the correctness of the threshold to prevent a peak of noise from growing near zero (if set too low) or from cutting the Compton (too high).

Calibration Coefficients The acquired spectrum has arbitrary units along the x-axis, therefore it needs calibration in energy. This procedure can be carried out for each detector in the following way: firstly it is necessary to fit the two peaks with a gaussian curve to find the centroid value $\mu_{1,2}$ for each (x coordinates of the peaks) and finally perform a linear fit of the two points $(\mu_1, 511 \text{ keV})$ and $(\mu_2, 1275 \text{ keV})$. The new calibrated values (energy in keV) can be extracted from the simple relation:

$$E_{\text{keV}} = a + b \cdot E_{\text{a u}} \qquad \begin{cases} a = \text{intercept} \\ b = \text{slope} \end{cases} \tag{1}$$

The parameters of the gaussian fits and the resolution R of the peaks for the spectrum of each detector are reported in Table 1. The values of intercepts and slopes of the calibration are stored in Table 2. The energy spectra and the graphs of the calibration are reported in Appendix A.

	μ_1 [a u]	FWHM$_1$ [a u]	R_1	μ_2 [a u]	FWHM$_2$ [a u]	R_2
D1	4530 ± 10	2030 ± 90	0.45 ± 0.02	12160 ± 40	3900 ± 100	0.32 ± 0.01
D2	2710 ± 4	1410 ± 10	0.520 ± 0.005	7010 ± 30	3000 ± 200	0.43 ± 0.02
D3	3091 ± 3	1298 ± 7	0.420 ± 0.002	7870 ± 20	2310 ± 50	0.293 ± 0.006
D4	1619 ± 1	575 ± 5	0.355 ± 0.002	4143 ± 7	1170 ± 20	0.282 ± 0.005
D5	2311 ± 2	893 ± 7	0.386 ± 0.003	5940 ± 10	1460 ± 50	0.246 ± 0.007
D6	1951 ± 2	685 ± 5	0.351 ± 0.002	4986 ± 8	1040 ± 20	0.208 ± 0.004
D7	1712 ± 3	1150 ± 10	0.671 ± 0.006	4120 ± 8	2600 ± 200	0.63 ± 0.06
D8	2654 ± 4	1330 ± 20	0.500 ± 0.006	6810 ± 10	1670 ± 50	0.246 ± 0.006

Table 1: Parameters and resolution of the gaussian fits for the calibration.

Detector	a [keV]	b [keV/a u]
1	57 ± 1	0.1001 ± 0.0002
2	29 ± 2	0.1777 ± 0.0003
3	17 ± 2	0.1599 ± 0.0003
4	21 ± 2	0.3027 ± 0.0006
5	24 ± 2	0.2105 ± 0.0004
6	20 ± 2	0.2517 ± 0.0005
7	-32 ± 2	0.3173 ± 0.0006
8	23 ± 2	0.1838 ± 0.0003

Table 2: Calibration Coefficients.

Some final considerations should be done:

- the 1275 KeV peak was difficult to identify in the most 'external' detectors, such as D2, D7, D8, than in the central ones, such as D3, D4, D5 and D6, where better results have been gained.
- The D7 spectrum is too noisy to be accepted: probably this fact is due to a defect of the detector itself.

4 Measurement of the mass attenuation coefficient

We chose to measure the mass attenuation coefficient of five different materials, whose samples had the shape of rectangular layers of different width, as shown in Table 3.

Material	Density [g/cm^3]	Width [cm]
Aluminum	2.699	2.0
Lead	11.35	0.5
Polyethylene	0.93	2.0
Iron	7.874	1.0
Graphite	1.7	2.0

Table 3: Material samples: density and width.

Data Acquisition We collected the energy spectra on detectors from D2 to D8 using the following logical condition:

$$\text{D1 } \textbf{AND } (\text{D2 } \textbf{OR } \text{D3 } \textbf{OR } \ldots \textbf{ OR } \text{D8}) \tag{2}$$

Such condition can be accomplished using the inverted signal of the detector D1 as inhibit and triggering on the OR signal of the detectors from D2 to D8. This is done in order to take all the measurements in coincidence.

First, we acquired spectra with no material between the radioactive source and the detectors, then the procedure was iterated for each of the samples listed in Table 3. In both cases the acquisitions lasted 30 minutes. Two typical energy spectra are shown in Figure 1 where it can be seen that they are made by:

- a very high peak at very low, almost null energies, which corresponds to the situation when a photon is detected by D1 in coincidence with one of the other detectors D2-D8, but not the one of these whose energy spectrum we are considering. In Figure 1 such part has been cut off, since it has a much higher statistics than the rest of the spectrum.
- The Compton part of the spectrum, corresponding to those photons which reached the detector and went out of it beacuse of Compton scattering.
- A peak after the Compton part, which corresponds to those 511 keV photons, which released all their energy in the detector.

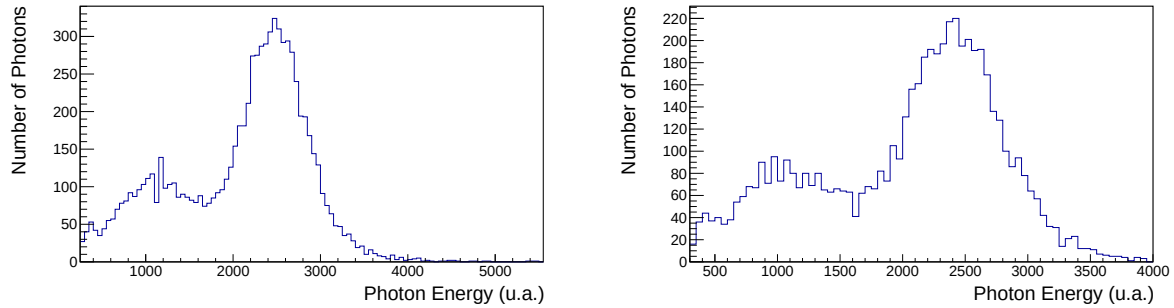

(a) No Material **(b)** Aluminium

Figure 1: Spectra acquired by detector 5

Watching the spectra taken at the most external detectors, it is easy to distinguish the null signal part from the rest, whereas it is difficult to identify the Compton edge and the 511 keV peak, due to the low statistics collected at those detectors. Energy spectra taken from detector 7 clearly suggest that a problem in data acquisition occured: it might be due to a defect of the detector itself or to a problem in the gain setting. For such reasons, we excluded the spectra acquired form detector 7 from our analysis.

Intensity and Mass Attenuation Coefficient Estimate In order to measure the intensities of the gamma rays collected at each detector, we decided to integrate the energy spectrum over a range such that it excluded the peak corresponding to null signals and contained the most non-null signals as possible. We hypothesized that the collection of a photon in such a range was a rare event, described by the Poisson distribution, and calculated the error on intensities as their square root:

$$I_{\text{material}} = N_{\text{photons}} \qquad \sigma_{I_{\text{material}}} = \sqrt{N_{\text{photons}}} \ . \tag{3}$$

After that, we computed the ratio between the intensites with and without the material:

$$R = \frac{I_{\text{material}}}{I_{\text{background}}} \qquad \sigma_R = R\sqrt{\left(\frac{\sigma_{I_{\text{material}}}}{I_{\text{material}}}\right)^2 + \left(\frac{\sigma_{I_{\text{background}}}}{I_{\text{background}}}\right)^2}\,. \tag{4}$$

Given R, we could calculate the mass attenuation coefficient μ:

$$R = e^{-\mu\rho\Delta x} \implies \mu = -\frac{\log R}{\rho\Delta x} \quad , \quad \sigma_\mu \simeq \left|\frac{1}{R\rho\Delta x}\right|\sigma_R \tag{5}$$

where ρ is the material density[1] and Δx is the width of the material. Both ρ and Δx are assumed to be exact values because they are known with a much better precision than R. At the end, we obtain a measurement for the mass attenuation coefficient for each detector (except D7) and each material, as shown in Table 4.

Detector	Aluminum	Lead	Polyethylene	Iron	Graphite
D2	0.048 ± 0.009	0.077 ± 0.009	0.11 ± 0.05	0.062 ± 0.007	0.04 ± 0.01
D3	0.038 ± 0.007	0.093 ± 0.007	0.05 ± 0.04	0.071 ± 0.005	0.04 ± 0.01
D4	0.065 ± 0.003	0.122 ± 0.003	0.096 ± 0.009	0.094 ± 0.002	0.068 ± 0.005
D5	0.063 ± 0.003	0.128 ± 0.003	0.113 ± 0.009	0.093 ± 0.003	0.071 ± 0.005
D6	0.064 ± 0.003	0.124 ± 0.003	0.114 ± 0.008	0.091 ± 0.002	0.061 ± 0.005
D7	***	***	***	***	***
D8	0.046 ± 0.007	0.103 ± 0.008	$-0.17^{***} \pm 0.04$	0.074 ± 0.005	0.06 ± 0.01

Table 4: Attenuation Mass Coefficients μ [cm^2/g].

We should notice the presence of a negative attenuation coefficient: it might be due to the low statistics of events acquired at external detectors, which made the measured intensity sensitive to background fluctuations.

Discussion From Table 4, it is possible to see that the mass attenuation coefficient varies as a function of the detector. In general it happens that μ is lower for the upper detectors D2, D3 and the lowest one D8, whereas it has higher values for the centrally positioned detectors D4, D5 and D6. This is evident from the plot in Figure 2.

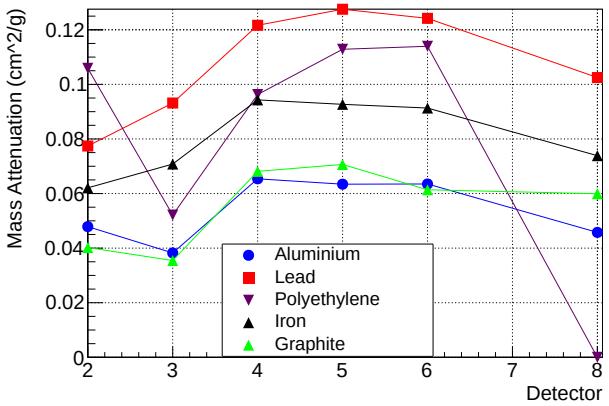

Figure 2: Mass Attenuation *vs* Detector.

[1]Densities are taken from `https://www.nist.gov/pml/x-ray-mass-attenuation-coefficients`

We tried to give an explanation for this behaviour of the mass attenuation coefficient as a function of the detector. Given that most of the photons are in the beam hitting the central detectors, we hypothesized that when a material is placed between source and detector, some of the 'central' photons undergo Compton scattering in the material, reach the side detectors and increase the intensity revealed at them. Such effect might have an influence in the attenuation coefficient taken at side detectors, because of the low number of signals collected by them. However, it should be pointed out that this is just an hypothesis which needs to be proved with further investigations.

In order to get a final estimate for the mass attenuation coefficient, we averaged all the values obtained in the various detectors, using the square inverse of errors as weights. Results are exposed in Table 5 and compared to the reference values[2] through the deviation

$$\frac{\delta\mu}{\mu} = \frac{\mu^{\text{average}} - \mu^{\text{reference}}}{\mu^{\text{reference}}} \tag{6}$$

and the gaussian compatibility

$$\lambda = \frac{|\mu^{\text{average}} - \mu^{\text{reference}}|}{\sigma_{\mu^{\text{average}}}}. \tag{7}$$

	Aluminum	Lead	Polyethylene	Iron	Graphite
μ^{average} [cm^2/g]	0,061 ± 0,002	0,121 ± 0,002	0,107 ± 0,005	0,090 ± 0,001	0,064 ± 0,002
$\mu^{\text{reference}}$ [cm^2/g]	0,0845	0,161	0,099	0,084	0,087
$\frac{\delta\mu}{\mu}$ %	-28 %	-25%	8%	7%	-26 %
Compatibility λ	15,4	24,9	1,5	5,4	10,1

Table 5: μ: Final Estimates *vs* Reference Values.

Our estimate was successful only for iron and polyethylene. However, even in the cases in which the two tests have negative outcome, we managed to estimate the order of magnitude of the mass attenuation coefficient. Given the approximate nature of our method, this can be considered a satisfying result.

5 Black box content reconstruction

In the last part of the experience, we tried to reconstruct the content inside a black box. In order to accomplish this objective, the box was diveded into five slices to be scanned separately, each one corresponding to a certain position of the motorized slide.

Data Acquisition An acquisition of 20 minutes was done for every position and for the background condition of no box in front of the detectors. In Table 6 the five positions from the previous one are reported., starting from a 'home' location.

[2]The reference values are taken from `https://www.nist.gov/pml/x-ray-mass-attenuation-coefficients`

Position	Steps
1	Right 21500
2	Right 10500
3	Right 10500
4	Right 10500
5	Right 10500

Table 6: Positions of the black box.

The acquisition was done with the same logic configuration explained in the previous Section in order to have an estimate of the attenuation ratio $R = I/I_0$ between the intensities with and without the i^{th} slice of the black box. In principle, if the slice contains a piece of a certain material, this information should be visible as R significantly smaller than 1. Moreover, the information given by i^{th} detector in the j^{th} position can be translated into the (i,j)-pixel of 7×5-pixel image, namely a matrix.

Data Analysis The analysis strategy consists in evaluating the number of photons incoming to a certain detector, excluding the null counts in the first channels, through the integral in a defined spectrum range. In Table 7 is reported the integral ratio I/I_0 for every case. The relations employed for the computation of R and the associated uncertainty are the same as in the previous Section.

Detector	Position 1	Position 2	Position 3	Position 4	Position 5
D2	1.02 ± 0.09	1.12 ± 0.09	0.57 ± 0.06	1.02 ± 0.09	1.15 ± 0.09
D3	1.05 ± 0.05	1.10 ± 0.05	0.55 ± 0.03	1.03 ± 0.05	0.97 ± 0.04
D4	0.97 ± 0.02	1.01 ± 0.02	0.42 ± 0.01	0.99 ± 0.02	0.99 ± 0.02
D5	0.95 ± 0.02	1.01 ± 0.02	0.44 ± 0.01	0.99 ± 0.02	0.98 ± 0.02
D6	1.00 ± 0.02	1.02 ± 0.02	0.43 ± 0.01	1.01 ± 0.02	0.99 ± 0.02
D7	0.99 ± 0.02	0.98 ± 0.02	0.42 ± 0.01	0.96 ± 0.02	0.98 ± 0.02
D8	1.09 ± 0.05	0.64 ± 0.03	0.60 ± 0.03	0.58 ± 0.03	0.95 ± 0.05

Table 7: Value of integral ratio for every case and every detector.

By putting this values in a matrix and plotting it as a 2D-histogram, a raw picture of the object comes out and it is reported in Figure 3.

Discussion What we see from this reconstruction is that the black box is likely to contain two rectangular shapes, one put vertically in the third slice and from D2 to D7, one put horizontally from slice 2 to slice 4 and in the zone scanned by D8. Concerning the material, the attenuation ratio observed in the pixels covered by the two shapes is compatible with the presence of 5 mm of lead. Another possibility is that the material can be 1 cm of iron, but it is not compatible with the physical dimensions of the black box.
Another important detail to highlight is that for some pixels the value of R results slightly greater that 1, which is due to the absence of obstacles inside the black box and for statistical fluctuations in the count of photons.

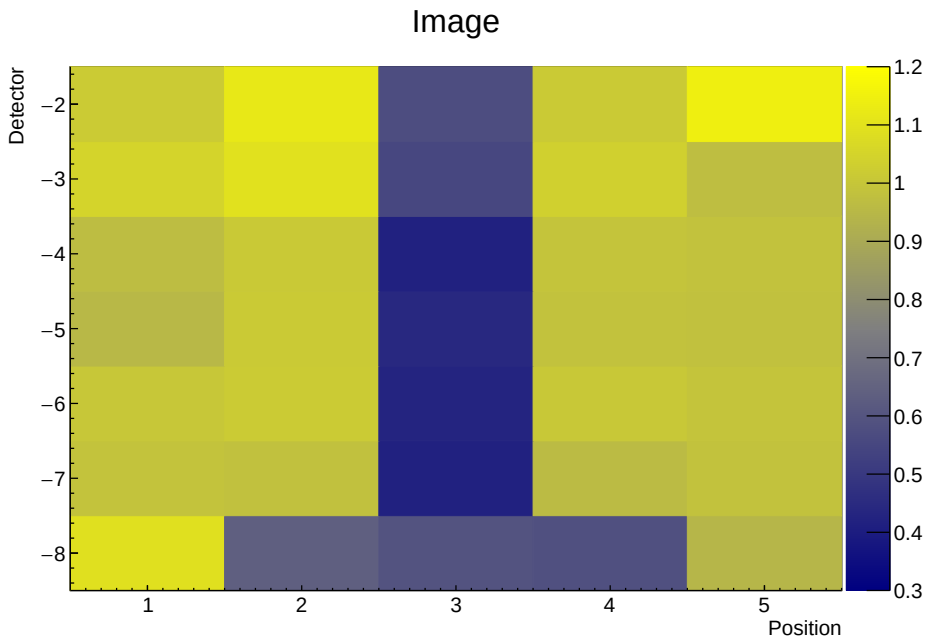

Figure 3: Reconstruction of the content inside the black box.

6 Conclusion

Our method for estimating the mass attenuation coefficient μ turned out to be a good tool to have a rough and rapid estimate of the order of magnitude of μ. Instead, it did not succeed in giving us an accurate estimate of the value of such parameter.
Concerning the construction of the image of the unknown object in the black box, our protocol was fully succesful, allowing us to clearly distinguish whether one of the pixels is observing the object or not. Its limit lies in the fact that it is not possible to determine the material composition of the object without knowing the width of its components, and viceversa.

A Calibration: energy spectra and regression fits

Spectrum acquired by detector D1

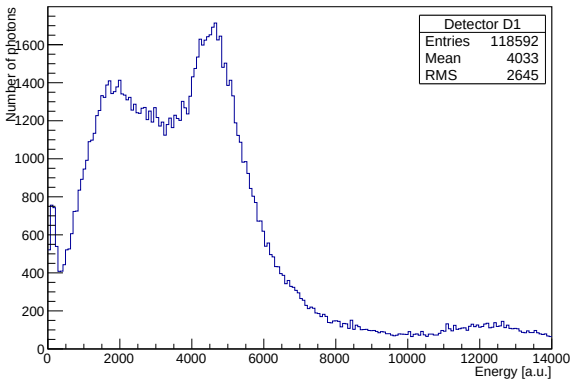

Calibration of detector D1

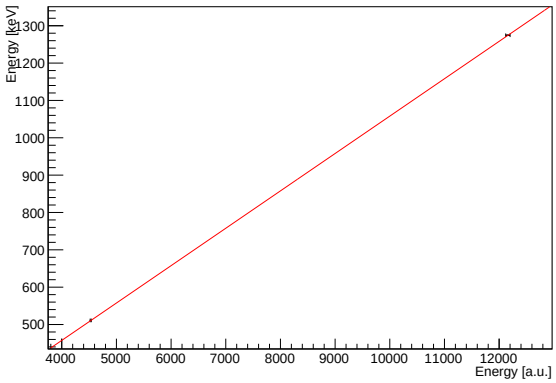

Spectrum acquired by detector D2

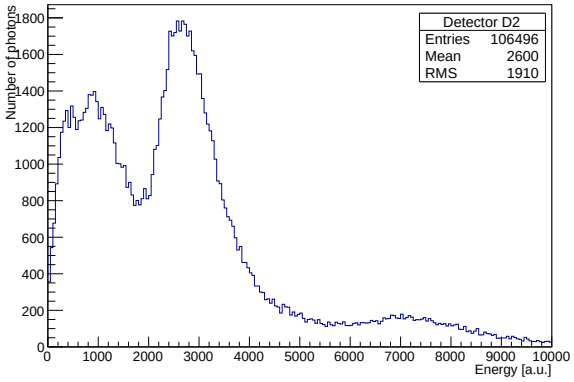

Calibration of detector D2

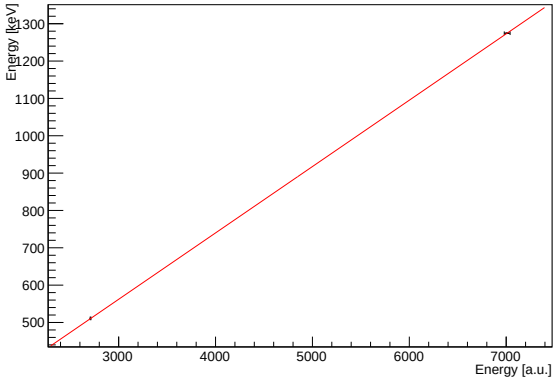

Spectrum acquired by detector D3

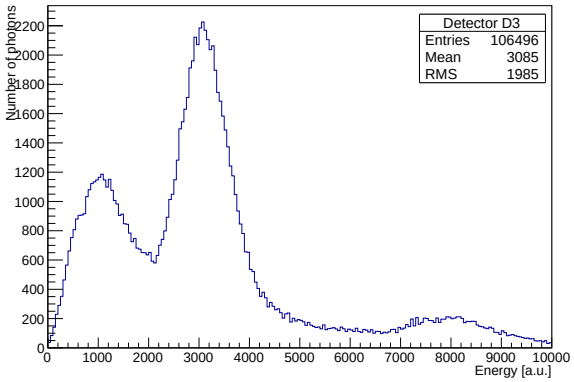

Calibration of detector D3

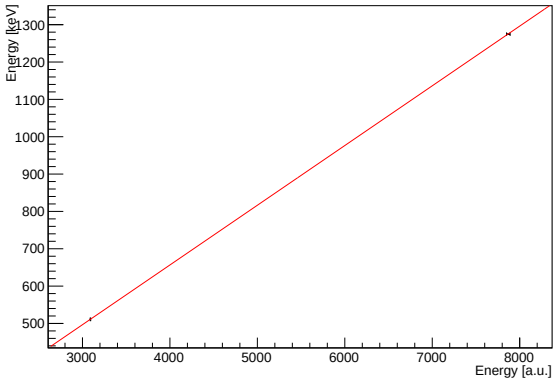

Spectrum acquired by detector D4

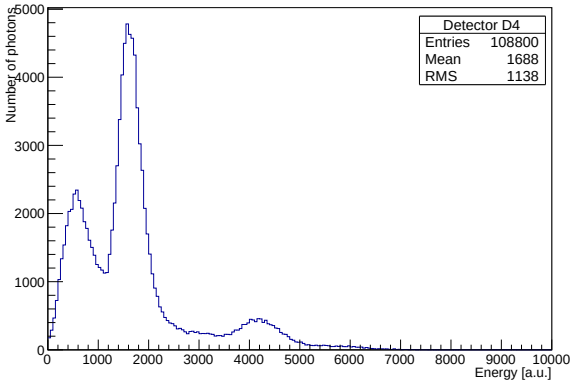

Calibration of detector D4

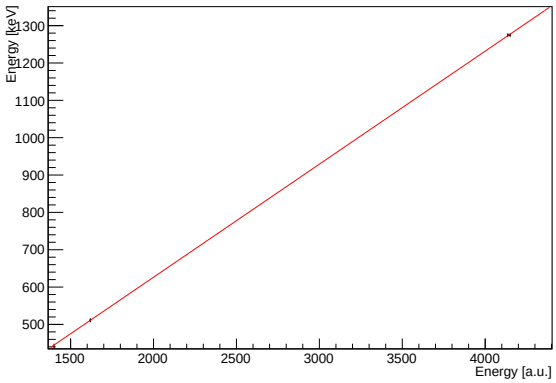

Spectrum acquired by detector D5

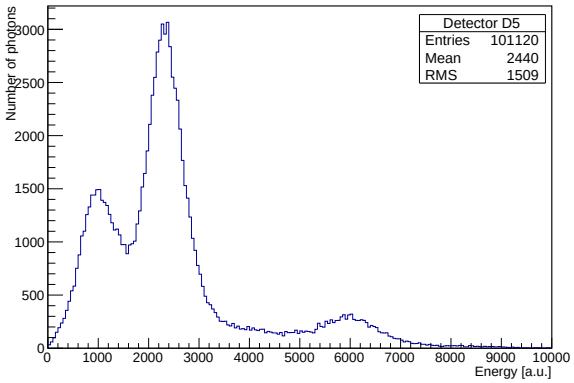

Calibration of detector D5

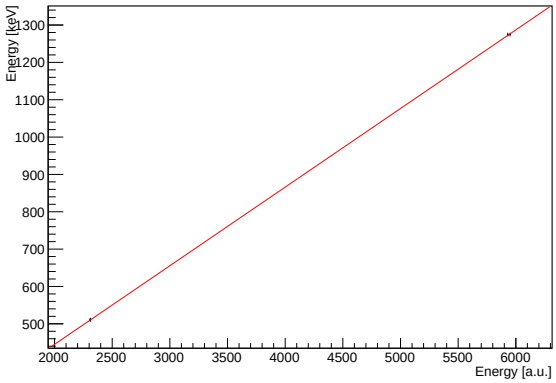

Spectrum acquired by detector D6

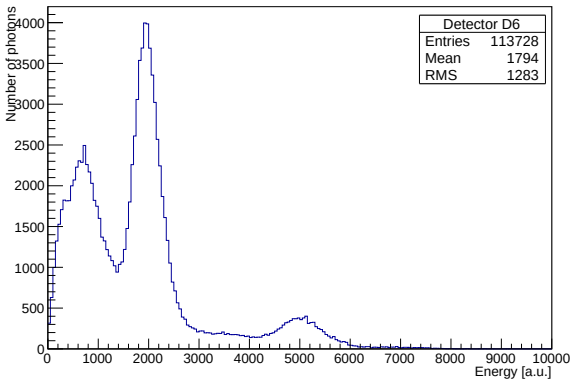

Calibration of detector D6

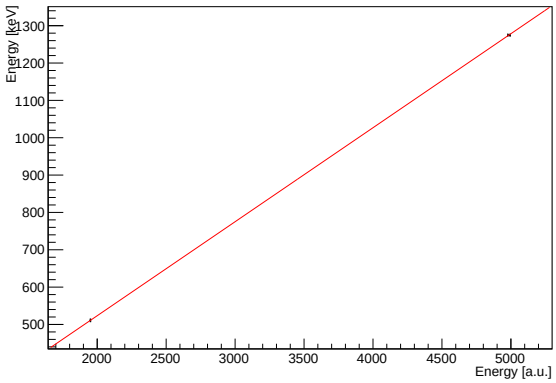

Spectrum acquired by detector D7

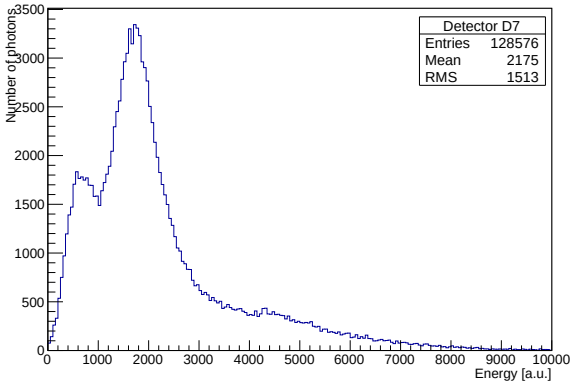

Calibration of detector D7

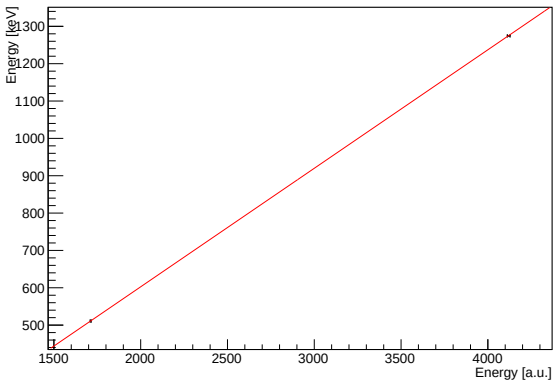

Spectrum acquired by detector D8

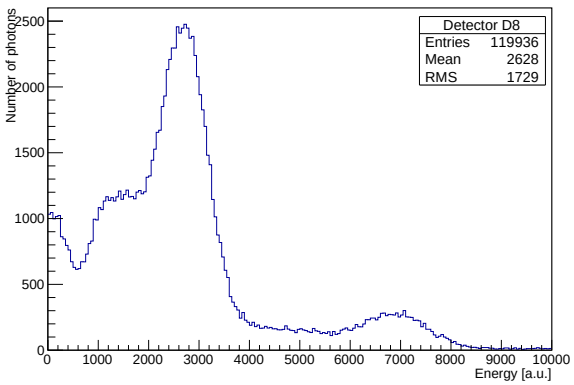

Calibration of detector D8